frontiers

Spots and flares in hot main sequence stars observed by *Kepler, K2* and *TESS*

L. A. Balona

South African Astronomical Observatory, P.O. Box 9 Observatory 7935, Cape Town, South Africa

Correspondence*:
Corresponding Author
lab@saao.ac.za

ABSTRACT

About 22000 *Kepler* stars, 7000 *K2* stars and nearly 60000 *TESS* stars from sectors 1–24 have been classified according to variability type. A large proportion of stars of all spectral types appear to have periods in their light curves consistent with the expected rotation periods. A previous analysis of A- and late B-type stars suggests that these stars are indeed rotational variables. In this paper we have accumulated data to show that rotational modulation is present in about 30–40 percent of A- and B-type stars. A search for flares in *TESS* A- and B-type stars resulted in the detection of 102 flares in 57 stars. Analysis of flare energies show that the source of the flares cannot be a cool dwarf companion nor a F/G giant. The realization that a considerable fraction of A- and B-type stars are active indicates that a revision of current concepts regarding hot star envelopes is required.

Keywords: stellar activity, stellar rotation, starspots, flare stars.

1 INTRODUCTION

Spots on stars other than the Sun were first discovered by Kron (1947). Following the work of Hall (1972), it is now well established that starspots similar to those in the Sun are present in stars with convective envelopes (Strassmeier, 2009). The presence of starspots leads to a brightness variation from which the rotation period can be found. Many thousands of solar-like stars with photometric rotational modulation have been detected from the *Kepler* space mission (McQuillan et al., 2013, 2014; Reinhold et al., 2013; Nielsen et al., 2013).

The rotational light modulation that is seen in cool stars with spots has never been detected in A- or B-type stars from ground-based photometry. However, high-precision space photometry of upper main sequence from the *Kepler* and *K2* missions show periodic or quasi-periodic light variations with periods consistent with the expected rotational periods of these stars (Balona, 2013, 2016, 2017). These studies were confined to A- and late B-type stars since only a small number of early B-type stars were observed by *Kepler* and *K2*. Balona (2019) extended the study to mid B-type stars using *TESS* Sectors 1–13. It appears that about 40 percent of A-type stars (Balona, 2013) and about 30 percent of mid and late B-type stars (Balona, 2019) are rotational variables. However, from a much smaller sample, Sikora et al. (2020) estimates that the incidence of chemically normal rotational variables might be less than 30 percent. High-resolution spectroscopic time series of Vega (A0V) also indicates the presence of a spotted stellar surface

(Böhm et al., 2015), providing independent confirmation of the photometric results. Savanov (2019) confirms the rotational character of the light variations in the A star, KIC 7047141. In this work we add further stars from *TESS* sectors 14–24, which now allow the rotational analysis to be extended to early B-type stars. Evidence for rotational light modulation among O stars has been presented by Buysschaert et al. (2015).

Flares on the Sun and cool stars are thought to be a result of energy release through the magnetic reconnection process. It is therefore natural to associate the presence of starspots with flares since both arise from localized magnetic fields on the surface. Flares on K and M dwarfs are well documented since their discovery by Luyten (1949). The advent of the *Kepler* space mission (Borucki et al., 2010) led to the discovery of flares on several F- and A-type stars (Balona, 2012) and superflares on solar-type stars (Maehara et al., 2012). Further studies (Balona, 2013, 2015; Balona et al., 2016b) indicate that around 2.5 percent of A-type stars flare with energies in the range 10^{35}–10^{36} erg. Švanda and Karlický (2016) find that of occurrence frequencies of stellar flares in A stars is systematically shifted towards a high-energy tail compared to stars of cooler spectral types. Pedersen et al. (2017) have argued that flares in A stars are likely a result of cool flare stars in the same aperture or binary companions. Direct evidence of possible X-ray flares in A-type stars have been reported by Schmitt et al. (1994), Robrade and Schmitt (2010), while a flare on a B-type star has also been reported (Yanagida et al., 2004, 2007).

Rotational modulation and flares in A- and B-type stars implies the presence of surface magnetic fields. According to current views, magnetic fields in stars are either of fossil origin (i.e. the star was born with an embedded global magnetic field), or are generated by the dynamo effect in mass motions that occur in convective layers (Parker, 1955; Charbonneau, 2014). Fossil fields are used to account for the strong global magnetic fields in Ap and Bp stars (Mestel, 1967; Braithwaite and Spruit, 2004). Since the outer envelopes of A- and B-type stars lack the deep convective layers in the Sun and cool stars, it has long been assumed that most A- and B-type stars do not possess surface magnetic fields. However, recent improvements in technology have resulted in the detection of very weak global fields in some bright A-type stars such as Sirius and Vega (Petit et al., 2011) and on Am stars (Blazère et al., 2016b,a).

Stellar pulsation in upper main sequence stars also challenges our current concepts of the outer layers of A- and B-type stars. First results from the *Kepler* space mission on pulsations in main-sequence A-type stars (Grigahcène et al., 2010) already indicated a serious problem. It turns out that nearly all δ Scuti stars have multiple low frequency pulsations which cannot be explained by current models (Balona, 2014, 2018). A further surprise was the confirmation that many late B-type stars pulsate with high frequencies (Maia variables, Balona et al. 2015, 2016a; Balona and Ozuyar 2020a). It does not seem possible to understand the pulsational instability of Maia variables as a consequence of incorrect opacities (Daszyńska-Daszkiewicz et al., 2017). Perhaps of even more significance is the fact that less than half of the stars in the δ Sct instability strip pulsate. Also, it seems that the γ Dor variables may be just a subset of the δ Sct stars (Balona, 2018). None of these findings are explained by current pulsation models which may perhaps be a result of incorrect assumptions regarding the outer layers of A- and B-type stars.

New ideas regarding the outer layers of stars in radiative envelopes have recently emerged. It has been suggested, for example, that generation of magnetic fields by dynamo action may occur in sub-surface convective zones in A- and B-type stars (Cantiello et al., 2009; Cantiello and Braithwaite, 2011, 2019). At the surface they give rise to bright starspots. Also, it has been suggested that differential rotation may act to provide dynamo-generated magnetic fields in radiative zones (Tout and Pringle, 1995; Spruit, 1999, 2002; Maeder and Meynet, 2004). Whether or not these ideas may offer a solution to the detection of

starspots and flares in A- and B-type stars, or help in resolving the challenges posed by pulsation, remains to be seen.

In this paper we report on further evidence for photometric rotational modulation among *TESS* A- and B-type stars, indicating that starspots are common among all B-type stars, including early B-type stars. We also report on a search for flares in *TESS* stars on the upper main sequence. On the basis of these results and the difficulty in explaining stellar pulsation in A- and B-type stars, we argue that current ideas regarding the outer layers of stars in radiative equilibrium need to be revised.

2 DATA AND METHODOLOGY

In searching for rotational modulation, the full four-year light curves from long cadence (30 min) *Kepler* data, together with light curves from *TESS* (2 min cadence) sectors 1–24 were used. In both cases light curves using pre-search data conditioning (PDC) were selected (PDCSAP_SAP flux column in the FITS file). These are corrected for time-correlated instrumental signatures (Jenkins et al., 2016). In addition stars from the *K2* mission (30 min cadence) were included.

In constructing the light curves, the mean was subtracted from each flux measurement and the result divided by the mean and multiplied by 1000 to covert to parts-per-thousand (ppt). No corrections or rejection of data points were made and the data quality was not taken into account. Neither was there any attempt to smooth the data or adjust the zero points between quarters/sectors. The PDC data, exactly as given in the FITS files, were used. These are sufficient for identifying the rotation period which is typically only a few days and most often in the range 0.5–3 d in these rapidly-rotating stars. All stars with effective temperatures $T_{\rm eff} > 6000$ K brighter than magnitude 12.5 in the V band were selected. There are 5643 *Kepler* and *K2* stars and over 50000 *TESS* stars in this temperature range. As already mentioned, the data for the *Kepler* and *K2* rotational variables have been described and published in (Balona, 2013, 2016, 2017). Many new *TESS* rotational variables were added to these in Balona (2019). The new *TESS* rotational variables added in this paper now include a sufficient number of early-B stars to show that rotational modulation is present even among the hottest B stars.

Visual inspection of the light curves and Lomb-Scargle periodograms (Scargle, 1982) of *Kepler*, *K2* and *TESS* stars were used to assign variability types whenever appropriate. The variability classification follows that of the *General Catalogue of Variable Stars* (GCVS, Samus et al. 2017). The only recognized class of rotational variables among the A- and B-type stars are the chemically peculiar α CVn and SX Ari classes. A new ROT class has been added to describe any star which is not known to be Ap or Bp and in which the light variation is suspected to be a result of rotation.

The main indication of a ROT variable is a significant peak in the periodogram at a frequency which might correspond to the rotation frequency. A significant peak is one in which the amplitude exceeds the background noise by a factor of four or more. This significance criterion is justified by simulations as discussed in Koen (2010). In practice, the ROT classification is assigned to any single, isolated peak with a frequency less than about $4\,{\rm d}^{-1}$. Sometimes the first harmonic is also present, which adds additional credibility to the identification. When the harmonic is present, it is the fundamental which is taken to represent the rotation frequency. It is possible that in some stars the fundamental might be missing or have very low amplitude, in which case the period will half the true period. This might occur in stars with two diametrically located spots of about the same size. It is not possible to identify such cases from the available data. Periods longer than about 20 d are somewhat uncertain due to the increasing noise level in the periodogram.

The ROT type can be confused with low-level eclipses. In general, the ROT identification is confined to stars with amplitudes less than 10 millimagnitudes in an attempt to avoid this possibility. Aided by suitable software, visual classification of over 100 stars an hour is possible. In this way, several thousand stars with $T_{\rm eff} > 6000$ K have been assigned the ROT type.

The work on stellar flares is not meant to be a comprehensive survey of flares in *TESS* early-type stars. The flares reported here are those visible in both the corrected (PDCSAP_FLUX) and uncorrected (SAP_FLUX) light curves without removing the underlying stellar variation (detrending). No doubt, many more such flares remain to be discovered. Only the *TESS* data are discussed because flaring in *Kepler* early-type stars has already been reported (Balona, 2012, 2013, 2015; Balona et al., 2016b). For this purpose, the selection was limited to about 14500 *TESS* stars with $T_{\rm eff} > 7500$ K. This temperature was chosen in order to select stars likely to possess radiative envelopes.

It is particularly interesting to detect flares in A- and B-type stars since these would not be expected to occur, but would be a natural consequence of surface magnetic fields associated with the active regions in a starspot. For this purpose, we do not confine the search criterion to ROT stars only. In stars where the brightness is rapidly increasing or decreasing, it is sometimes difficult to detect flares unless they are of large amplitude. In such cases detrending is often necessary to render the flares more visible. For this reason, stars known to vary on a short timescale, such as the large number of δ Sct and other rapid variables with large amplitudes, were not included in the search for flares. This reduces the sample of 14500 stars to 6072 A- and 1616 B-type stars.

3 STELLAR PARAMETERS

The most commonly used test for rotational modulation is comparison of the rotation rate derived from the photometric frequency, $\nu_{\rm ROT}$, with that derived from the projected rotational velocity, $v \sin i$. To derive the equatorial rotational velocity, v, from $\nu_{\rm ROT}$ requires an estimate of the stellar radius, R. This can be done if we know the effective temperature, $T_{\rm eff}$, and luminosity, $L/L_\odot$.

A catalogue of over 101500 stars comprising nearly 170000 individual $T_{\rm eff}$ measurements using various methods was compiled. For this purpose, the *PASTEL* catalogue (Soubiran et al., 2016) was very helpful, but many other references in the literature were searched. The most precise method of deriving $T_{\rm eff}$ is by modelling absorption line profiles from medium- or high-resolution spectroscopy. For A- and B-type stars, this involves fitting the Hβ and/or Hα line profiles because the strengths of the Balmer lines are sensitive to effective temperature. By comparing the observed line profiles with those generated by a suitable model atmosphere, the value of $T_{\rm eff}$ and $\log g$ can be directly measured. The resulting standard deviation in $T_{\rm eff}$ ranges from about 100 K for A-type stars to about 1000 K for early B stars. Spectroscopic estimates of $T_{\rm eff}$ exist for about 25 percent of the sample considered here.

The next best method is the use of narrow-band photometry. This involves measuring the strength of the Hβ line (the Strömgren β index) usually in conjunction with $uvby$ narrow-band photometry. The β index is sensitive to $T_{\rm eff}$, but a colour index is necessary to distinguish between A- and B-type stars. The value of $T_{\rm eff}$ is obtained either by direct comparison with synthetic photometry derived from model atmospheres or by using stars with known $T_{\rm eff}$ (Moon and Dworetsky, 1985; Gray, 1991; Napiwotzki et al., 1993; Smalley and Dworetsky, 1993; Balona, 1994). Estimates of $T_{\rm eff}$ from Sloan $ugriz$ (Brown et al., 2011) are of this type and are available for most of the *Kepler* stars. However, they cannot be used for stars earlier than A0 because they lack u-band measurements. Without the u band, it is impossible to distinguish between A- and B-type stars of the same colour. The same problem occurs with the majority of *TESS* effective temperatures for B-type stars. However, when these were in approximate agreement

Table 1. Number of ROT stars within the given $T_{\rm eff}$ range, $N_{\rm ROT}$. Also shown is the fraction of ROT stars, $f_{\rm ROT}$ within the range. $N_{\rm vsini}$ is the number of stars used to construct the $v \sin i$ vs v diagrams (Fig. 1).

$T_{\rm eff}$	$N_{\rm ROT}$	$f_{\rm ROT}$	$N_{\rm vsini}$
6000–7000	21835	0.50	3329
7000–8000	3298	0.34	239
8000–10000	2418	0.31	420
10000–12000	529	0.40	205
12000–18000	341	0.37	219
18000–30000	138	0.29	85

with $T_{\rm eff}$ estimated from the spectral type, the *TESS* value was used. Estimates of $T_{\rm eff}$ using narrow- and intermediate-band photometry are available for about 55 percent of stars.

If neither spectroscopy or narrow-band photometry is available, wide-band photometry can be used to estimate $T_{\rm eff}$ provided that the reddening is known. This method is used in 7 percent of our sample. Finally, if nothing else is available, a crude estimate of $T_{\rm eff}$ can be derived from the spectral classification together with suitable calibration such as the calibration of Pecaut and Mamajek (2013). This method was used for 18 percent of the stars.

The stellar luminosity is best estimated from *Gaia* DR2 parallaxes (Gaia Collaboration et al., 2016, 2018) in conjunction with reddening derived from a three-dimensional map by Gontcharov (2017) and the bolometric correction calibration by Pecaut and Mamajek (2013). From the error in the *Gaia* DR2 parallax, the typical standard deviation in $\log(L/L_\odot)$ is estimated to be about 0.05 dex, allowing for standard deviations of 0.01 mag in the apparent magnitude, 0.10 mag in visual extinction and 0.02 mag in the bolometric correction in addition to the parallax error.

Table 1 lists the number of stars classified as ROT variables in the given range of effective temperature. Also shown is the fraction of main sequence stars for which the ROT classification was assigned. Rotational modulation occurs in about 30–40 percent of A- and B-type stars. Note that Be stars were excluded from the sample. While the light variations in Be stars can be interpreted as rotational modulation, the light amplitude is typically an order of magnitude larger than for non-Be stars (Balona and Ozuyar, 2020b). It is suggested that the cause of the variability are co-rotating clouds which obscure a larger fraction of the photosphere than starspots. Because of the large amplitude, Be stars are disproportionately represented among the ROT stars. Since Be stars are rapid rotators, their inclusion leads to an over-estimate of the proportion of ROT stars with rapid rotation. Most Be stars are of early B type and this leads to a severe distortion of the velocity distribution for stars with $T_{\rm eff} > 18000$ K.

4 ROTATIONAL MODULATION

The photometric period, obtained from *Kepler/K2* and *TESS* light curves together with the stellar radius is used to estimate the equatorial rotational velocity, v. If the variability is rotational modulation, there should be a relationship between v and the projected rotational velocity, $v \sin i$. It is expected that the rotational axes are randomly orientated. In this case the probability of the rotational axis being inclined at angle i is proportional to $\sin i$. There will be a diminishing scatter of points below the $\sin i = 1$ line due to stars with lower angles of inclination. Due to unavoidable errors (e.g. uncertainties in $v \sin i$, in the interstellar reddening, in the bolometric correction, in the parallax, and in the effective temperature), the

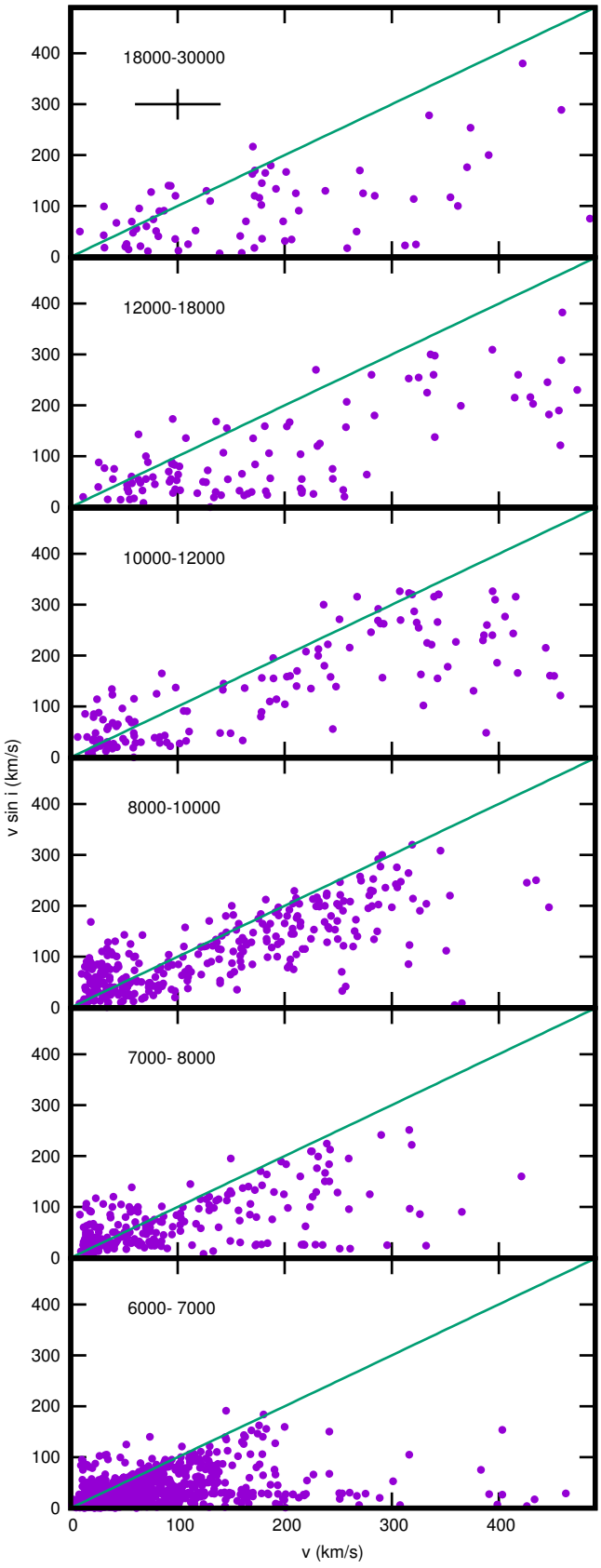

Figure 1. The relationship between the projected rotational velocity, $v \sin i$ and the equatorial rotational velocity, v (estimated from the photometric frequency), for different ranges of $T_{\rm eff}$ (labeled). The cross in the top left panel shows the estimated 1-σ error bars. The straight line corresponds to $v = v \sin i$. Be stars have been omitted.

resulting error in the stellar radius and the resulting equatorial rotational velocity is large, and it is to be expected that some points will lie above the $v \sin i = 1$ line.

A catalogue of projected rotational velocities, $v \sin i$ consisting of over 58000 individual measurements of 35200 stars was compiled. The bulk of these measurements are from Głębocki and Gnaciński (2005). The catalogue was brought up to date by a literature search. The typical error in $v \sin i$ can be estimated from the catalogue of Głębocki and Gnaciński (2005). The error increases with $v \sin i$ and ranges between 0 and 60 km s^{-1}. A representative value of $\sigma_{v \sin i} = 30$ km s^{-1} is reasonable. From the error in $\log L/L_\odot$ and $T_{\rm eff}$ it is easy to calculate the error in v. This error depends almost entirely on the error in $T_{\rm eff}$. The contribution from the luminosity error is small while the contribution from the error in the rotation period is entirely negligible. The typical value for the error in the derived equatorial rotational velocity is $\sigma_v \approx 40$ km s^{-1}.

Projected rotational velocities are not available for every star for which v has been estimated. In Fig. 1, the v–$v \sin i$ diagram is shown for all stars for which measurements are available. The data used to construct this figure are available as supplementary material. For completeness, *Kepler, K2* and *TESS* stars used in previous analyses and with available $v \sin i$ measurements are included. There are many previously unpublished stars with photometric periods, but without $v \sin i$ measurements. These will be published elsewhere.

The typical error bars discussed above are indicated in the top left panel. It is clear that the expected distribution of points is present from the F- to the early B-type stars. This justifies the original assumption that the periodic light variation is due to rotation.

As expected, nearly all stars with $v > 60$ km s^{-1} lie on or below the $\sin i = 1$ line. For low rotation rates, ever increasing observational precision is required to determine whether or not $v \sin i < v$. Often, $v \sin i$ values are truncated at some positive number corresponding to the resolution limit of the instrument. It becomes increasingly difficult to distinguish between binarity and rotation at low frequencies. For example, amplitude variability, which is a typical attribute of rotational modulation, is not so easily detected. Thus one may expect significant contamination from binaries at low rotation rates. These factors are probably responsible for the increased scatter in this region.

5 *TESS* EARLY-TYPE FLARE STARS

In our catalog of nearly 60000 *TESS* stars classified for variability, there are 14495 stars with $T_{\rm eff} > 7500$ K. As already mentioned, eclipsing binaries, δ Sct stars and other types of rapid variables with high amplitudes require detrending to render the flares visible. To avoid this complication, only non-varying or slowly-varying stars were selected in the search for flares. This results in 6072 A- and 1616 B-type stars in which the variability is not too rapid. Flares were detected by visual inspection of the light curves. The intention is not to detect every incidence of flares among the A- and B-type stars, but merely to show that such flares exist, as they do in the *Kepler* data.

A flare is taken to be an event consisting of a sharp rise and gradual fall in brightness. Flares of short duration (a few minutes) will be missed because the *TESS* observations have a cadence of 2 min. It is possible, of course, that an event similar to a flare would be generated by a passing object (satellite or minor planet). Indeed, some examples of such events are visible in the *TESS* light curves, but their shapes are different from what might be expected in a flare. If events looking like typical flares are present in many stars, it becomes less likely that these are generated by passing objects. In particular, if these events occur several times in the same star (as found in a few stars), the probability that these are extrinsic to the

Table 2. Flare stars detected from visual inspection of *TESS* light curves. The TIC number and star name is followed by the assigned variability class and rotation period, $P_{\rm rot}$, in days. The effective temperature, $T_{\rm eff}$ (K), luminosity, $\log \frac{L}{L_\odot}$ and spectral type are also shown. Many stars appear to be X-ray sources as given by the literature reference. Finally, the spectral type is shown.

TIC	Name	Type	$P_{\rm rot}$	$T_{\rm eff}$	$\log L/L_\odot$	ref	Sectors	Sp.Type
11201915	HD 37410			7966	1.26	1	6	kA4hA2VmA7
11895653	HD 103287			9354	1.80	2	15,21,22	A1IV(n)
22562087	HD 107143	ROT	2.924	8234	1.20		10	A1V
25424318	HD 111608	ROT	0.874	9155	1.40		10	A1IV
26893151	HD 11060	ROT	1.460	8494	1.18	3	17	A0
28643592	HD 174830	ROT	3.279	7953	1.63		14	A2
29671013	HD 200052			8892	1.47		1	A5V:pSiMg
30052567	HD 76516	ROT	0.329	8971	1.42		8	A0V
34404183	HD 152384	ROT	0.345	9096	1.55		12	A0V
50624799	HD 36118	ROT	0.742	11183	1.80	4	6	B9V
55219038	HD 43620	ROT	4.425	8476	1.43		19,20	A2
75873633	HD 133574	ROT	0.466	7078	0.92		11	A9/F0V
92136299	HD 222661	ROT	0.444	10618	1.73	5	2	B9.5IV
125958765	HD 154426	ROT	0.309	7915	1.24	3	12	A7III
142268253	HD 16754	ROT	3.817	8997	1.40	2	3	A1Va
142457761	HD 90759			8778	1.12		14,20,21	A2
147622676	HD 94660	ACV	2800	9544	1.77	3	9,10	A0pEuCrSi(Sr)
150125205	HD 29646	ROT	4.016	9594	1.76	3	19	A1IV
150250959	HD 44532	ROT	2.865	8072	1.21		2,3,5-10,12,13	A2V
177284702	HD 51581	DSCT		7266			7,9-13	A8V
199752613	HD 35885	ROT	0.839	9566	1.09		6	A0
215256883	HD 17864	ROT	0.335	9542	1.48	3	3	B9.5V
220399820	HD 29578	ACV	0.975	7415	1.40		3,5,9	A5:pSrEuCr
233164000	HD 108346	ROT	3.030	9522	1.42		22	kA1hA9mF2
236003103	HD 195984	ROT	1.323	9900	1.50		18-20	A0V
248430494	HD 33190	ROT	5.988	15100	2.17		5	B8V
248992635	HD 33819		3.448	8735	1.26		5	A0V
252834311	HD 20842	ROT	3.448	9900	1.39		18	A0Va+
256749693	HD 191174	ROT	4.608	9170	1.40	2	14-18,21,24	A2II-III
260416268	HD 45229		2.257	7537	1.29	2	1-9,11-13	kA2hA7VmA7
264683456	HD 36030	ROT	5.714	8992	1.70	6	6	A0
280965566	HD 83719	EA/ROT	1.220	7992	1.81	3	9	A0V
284084463	HD 22961	ACV	2.096	9650	1.37		18	A1pSr
287178418	HD 86001	ROT	3.185	7749	1.13		14,20,21	A2V
287329624	HD 57642	ROT	7.194	6900	0.84		1-13	A8IV/V
299899924	HD 54682	ROT	0.341	7404	1.50		1-13	A0V
301749125	HD 155056	ROT	3.650	9241	1.39		12,13	A2V
327136878	HD 9622	ROT	5.376	5978	0.64		17,18	A0pSi?
327724630	HD 209468	ROT	1.189	8906	1.48		1	A1V
332659885	HD 26624	ACV	0.340	7960	1.14		5	A2/3V
349193923	HD 56911	ROT	7.353	9624	1.47		1,3-11,13	A0Vs
352939640	HD 25553	ROT	1.650	9900			19	A0V
358467237	NGC 2516 4	ROT	1.019	6379	0.95	7	1,4,7-11	A7III
360020620	HD 190833	GDOR+ROT	0.568	9900	1.28	3	14-26	A0V
393389739	HD 43881	ROT	0.403	9123	1.32		6,7	A2V
395007683	HD 97049	ROT	0.745	9034	1.19		11,12	A2V
404477098	HD 15527	ROT	0.540	6929	1.22		4	A9V
407825808	HD 163837	ROT	1.536	7023	0.83	8	12,13	A9V
426452677	HD 143474	ROT	0.814	7620	1.29	2	12	A5IVs
427393202	HD 294262	ROT	1.041	6962	1.71	3	6	A0:
427458366	HD 290674	ROT	6.061	8416	1.53		6	A0V
438598966	HD 116649	ROT	1.055	8200	1.22		11	A0V
440863421	HD 131885	ROT	3.636	8793	1.47		11	A0V
442926107	HD 35308	ROT	1.520	8631	1.42		5,6	A0V
443316662	HD 45341	ROT	5.076	7159	1.13		6	A2
452468734	HD 80950	ROT	16.129	10069	1.61		10-12	A0V
459786991	HD 82861	ROT	1.621	7537	1.29	3	21	kA2mF0

References:
1- Lo et al. (2014); 2 - Schröder and Schmitt (2007); 3 - Voges et al. (1999); 4 - Evans et al. (2013); 5 - Makarov (2003);
6 - Evans et al. (2019); 7 - Marino et al. (2006); 8 - Voges et al. (2000)

Table 3. List of individual flares for stars in Table 2. The time of peak flare intensity, $t_{\rm max}$, is relative to BJD 2457000. The flare energy, E (erg), and the logarithm of relative peak flare intensity, $\log \frac{\Delta F}{F}$ is shown. The flare rise time, $t_{\rm rise}$, and the e-fold decay time, $t_{\rm decay}$, are in hours.

TIC	$t_{\rm max}$	$\log E$	$\log \frac{\Delta F}{F}$	$t_{\rm rise}$	$t_{\rm decay}$	TIC	$t_{\rm max}$	$\log E$	$\log \frac{\Delta F}{F}$	$t_{\rm rise}$	$t_{\rm decay}$
11201915	1486.726	34.19	-2.52	0.20	0.30	287178418	1856.612	34.72	-2.06	0.10	0.37
11895653	1909.470	33.99	-2.83	0.10	0.41	287329624	1478.194	34.55	-2.35	0.17	0.54
	1911.933	34.20	-2.81	0.27	0.73	299899924	1488.605	35.07	-1.95	0.80	0.76
	1921.062	34.38	-2.76	0.13	0.99		1505.676	34.36	-2.07	0.03	0.19
22562087	1588.461	33.89	-2.50	0.07	0.13		1506.614	34.68	-2.03	0.20	0.35
25424318	1573.681	34.34	-1.98	0.07	0.12		1574.564	35.11	-1.67	0.10	0.43
26893151	1780.812	34.96	-2.23	0.23	1.37	301749125	1664.922	34.51	-2.28	0.13	0.37
	1781.182	34.03	-2.56	0.13	0.25		1669.847	34.19	-2.30	0.07	0.22
28643592	1689.399	34.28	-2.52	0.23	0.32	327136878	1814.033	34.18	-2.34	0.03	0.24
29671013	1336.795	34.31	-2.38	0.07	0.30	327724630	1341.538	33.80	-2.63	0.03	0.20
30052567	1538.249	34.77	-2.09	0.20	0.42	332659885	1452.087	34.06	-2.44	0.10	0.19
34404183	1648.005	35.00	-2.50	0.60	2.80		1454.182	34.08	-2.49	0.03	0.29
50624799	1489.781	35.06	-1.99	0.43	0.60	349193923	1521.062	34.38	-2.28	0.10	0.27
55219038	1862.376	34.19	-2.52	0.20	0.33		1585.539	34.32	-2.39	0.03	0.36
75873633	1618.675	34.69	-2.11	0.17	0.42	352939640	1827.236	35.02	-2.28	0.17	0.60
	1621.946	34.16	-2.37	0.07	0.27		1827.295	35.01	-2.22	0.10	0.73
92136299	1355.329	33.78	-2.78	0.03	0.27		1561.076	34.80	-2.15	0.27	0.54
	1371.661	33.51	-3.13	0.27	0.22	358467237	1333.981	35.38	-1.78	1.00	0.59
	1380.647	34.44	-2.63	0.37	0.67		1433.087	35.24	-1.59	0.33	0.33
125958765	1649.168	34.89	-1.98	0.37	0.38	360020620	1700.051	36.03	-0.97	0.27	0.61
142268253	1397.155	33.95	-2.92	0.27	0.38		1719.691	35.20	-1.91	0.40	0.94
	1401.710	33.92	-2.89	0.33	0.40		1736.091	34.89	-1.87	0.27	0.32
142457761	1683.611	34.57	-2.01	0.03	0.25		1772.673	36.00	-1.38	0.77	1.32
	1709.402	34.30	-2.27	0.03	0.25		1773.752	34.95	-1.89	0.20	0.48
147622676	1575.018	34.20	-2.59	0.10	0.42		1791.842	35.14	-1.85	0.23	0.62
150125205	1819.610	34.09	-2.69	0.13	0.45		1793.708	34.79	-2.06	0.27	0.45
150250959	1451.683	34.61	-2.09	0.07	0.37		1843.284	35.38	-1.73	0.37	0.84
177284702	1661.791	34.99	-1.73	0.27	0.22		1865.436	35.00	-1.83	0.43	0.39
199752613	1472.599	36.00	-1.31	1.40	1.08		1887.015	35.28	-1.68	0.07	0.65
	1485.648	34.65	-2.02	0.03	0.34		2007.692	35.12	-1.64	0.13	0.39
215256883	1400.628	34.49	-2.11	0.03	0.27	393389739	1493.712	34.43	-2.68	0.40	0.93
	1401.217	34.06	-2.88	0.40	0.57	395007683	1646.653	34.09	-2.23	0.03	0.13
220399820	1394.360	34.20	-2.25	0.03	0.20	404477098	1423.255	35.27	-1.50	0.30	0.27
233164000	1916.760	34.52	-2.49	0.27	0.63	407825808	1627.180	34.57	-2.10	0.20	0.35
236003103	1821.522	34.62	-2.35	0.27	0.60	426452677	1636.713	34.93	-2.06	0.13	0.70
	1856.797	34.29	-2.31	0.07	0.29	427393202	1478.452	35.28	-1.78	0.40	0.75
248430494	1447.912	34.04	-2.59	0.20	0.22	427458366	1481.908	34.54	-2.36	0.90	0.12
248992635	1453.518	34.30	-2.20	0.03	0.25	438598966	1608.599	34.38	-2.53	0.17	0.53
252834311	1804.068	33.90	-2.63	0.27	0.12	440863421	1616.471	33.63	-2.91	0.10	0.18
256749693	1699.388	34.30	-2.31	0.07	0.27		1616.885	34.23	-2.60	0.07	0.42
260416268	1336.892	34.11	-2.29	0.07	0.18	442926107	1444.451	34.67	-2.20	0.33	0.34
	1643.010	34.03	-2.54	0.03	0.28		1455.540	34.57	-2.43	0.50	0.74
	1469.440	33.55	-2.84	0.03	0.17	443316662	1474.244	34.10	-2.56	0.13	0.36
	1470.150	33.80	-2.73	0.03	0.24		1488.023	34.01	-2.51	0.03	0.25
	1472.880	33.99	-2.66	0.07	0.31	452468734	1592.160	33.55	-2.71	0.03	0.12
	1479.676	33.84	-2.63	0.03	0.21	459786991	1870.886	34.55	-2.52	0.77	0.40
	1479.676	33.85	-2.62	0.03	0.22		1873.079	33.94	-2.59	0.10	0.19
	1487.262	33.86	-2.67	0.23	0.19		1887.635	34.43	-2.41	0.27	0.43
264683456	1488.888	34.91	-2.11	0.24	0.73		1889.358	34.66	-2.59	0.63	1.19
280965566	1559.256	35.27	-1.85	0.40	0.76		1889.875	33.75	-2.82	0.30	0.21
284084463	1810.223	34.82	-2.09	0.20	0.50		1892.900	34.08	-2.42	0.23	0.22

star is negligible. If the events are due to some instrumental problem, then they should occur at the same time on a given CCD chip or possibly on the entire ensemble of chips, depending on the problem. No instance of two or more flares occurring at the same time was found. Nevertheless, it cannot be excluded that some events identified as flares may be due to other causes.

The 57 stars in Table 2 appear to have at least one flare-like event. In this table the stellar parameters are shown. A substantial proportion of the flare stars are X-ray sources. Table 3 gives information on all flare-like events that were detected. The rise time, $t_{\rm rise}$ is the time taken for the flare to reach maximum intensity, while $t_{\rm decay}$ is the time from maximum intensity to the time when the intensity reaches 1/e of its maximum value (the e-folding time). In deriving these values, the flare background was removed by fitting a polynomial of low degree or, in some cases, by fitting a spline curve.

Examples of flares are shown in Fig. 2. Multiple flares are visible in 21 stars, giving a total of 102 flare events. Not included here are the *TESS* A-type flare stars TIC 118327563 and TIC 224244458 (Balona et al., 2019a). The former is a sdB star and the latter is an SX Ari variable (Bp star). Also excluded is the δ Sct flare star TIC 439399707 (Balona et al., 2019b) and the Be X-ray source TIC 207176480 (Balona and Ozuyar, 2020b).

The number of *TESS* A-type stars which appear to flare constitute about 1 percent of the sample of A-type stars which were examined, which is less than half of the 2.5 percent flare incidence among *Kepler* A-type stars reported by Balona (2013) and Balona (2015). This can be understood given the fact that the long-cadence *Kepler* data span four years, while the *TESS* data mostly span a few months and always less than one year. There are 61 *Kepler* A-type stars known to flare (Balona, 2015). The additional 57 flare stars reported here do not include any of the *Kepler* stars, bringing the total of flaring A-type stars to 118.

Because the stellar continuum is very weak in the UV, flare amplitudes in cool dwarfs increase very rapidly towards the UV. The *TESS* photometric pass band is 6000–11000 Å where flare emission is much lower and the stellar continuum much higher. This means that cool star flare amplitudes observed by *TESS* are very much lower compared with observations in the blue and UV. Any cool star in the aperture would need to be of comparable brightness to the A star for the flare to be detected. Whereas the continuum of a cool star in the near infra-red is relatively brighter than that of an A star of the same visual magnitude, the flare amplitude will be lower. Therefore the flare visibility would probably not be greatly affected whether the the relative magnitude difference is measured in the visual or in the near infra-red.

Whereas the *Kepler* pixel size is 4 arcsec, the *TESS* pixel size is 21 arcsec. This means that the probability of a flare originating in a star other than the A star is much larger for *TESS*. The stars are all very bright (4.2–10.4 mag), with most in the range 6–8 mag. The fields of all 57 stars were examined using the 2MASS, DSS images in SIMBAD. In every case the A star is by far the dominant optical source and no companion of significant brightness was found within a radius of 1 arcmin. The *Gaia* database (Gaia Collaboration et al., 2016, 2018) was examined for stars within a radius of 1 arcmin, but none brighter than about 12.5 mag was found. TIC 256749693 and TIC 360020620 are close doubles with magnitude differences of 3.2 and 1.7 mag respectively.

A search for foreground cool dwarfs was made using the catalogue of Muirhead et al. (2018) which lists over 1 million of these stars. Only three A-type stars were found where a cool dwarf was present within a radius of 2 arcmin. None of these cool dwarfs was brighter than 14.4 mag (the minimum magnitude difference being 6.5 mag). It is thus very unlikely that a cool dwarf is the source of the flare in any of the A-type stars. Therefore the flares must be due to exotic faint objects, a physical companion of the A star or the A star itself.

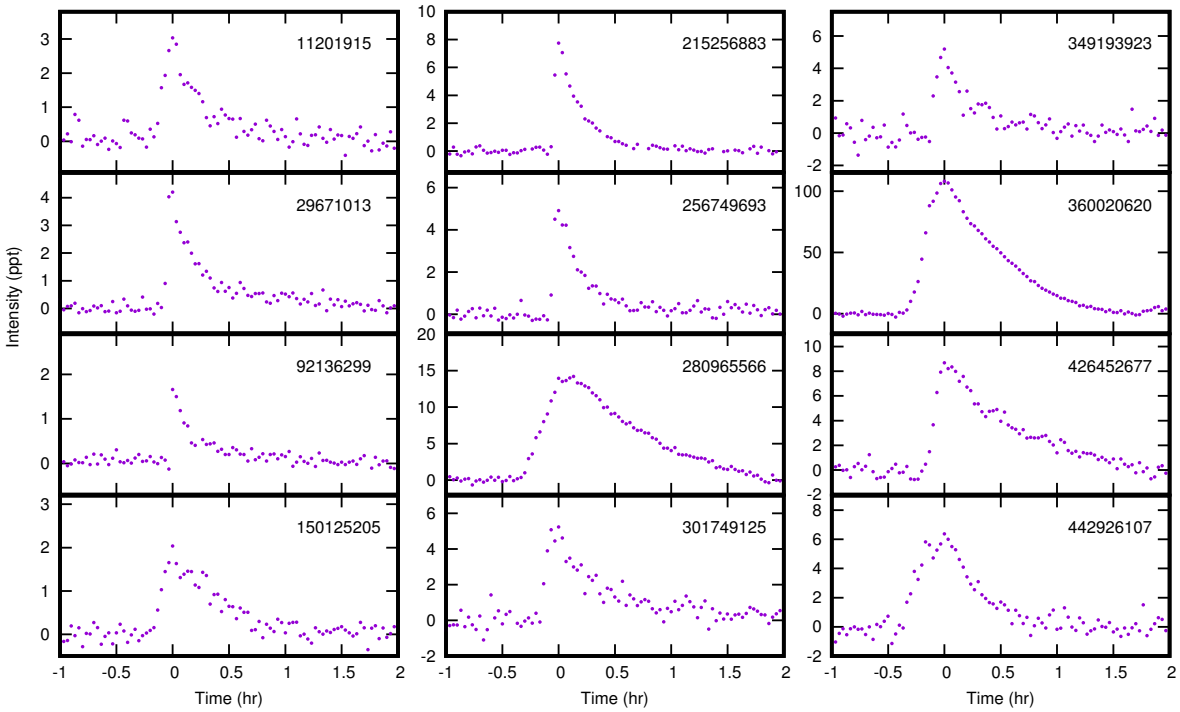

Figure 2. Examples of A star flares in the *TESS* data. The time origin is the time of maximum flare intensity. Time is in hours and intensity if parts per thousand.

The flare energy was estimated by integration of the flare light curve. From the estimated stellar luminosity the energy radiated by the flare can then be determined. This assumes that the wavelength distribution of flux from the flare is about the same as from the star. If the flux distribution in the flare corresponds to a blackbody with temperature higher than about 10 000 K, the true energies will be larger. Thus Schmitt et al. (2019) adopt a blackbody flux distribution corresponding to 12 000 K, while Froning et al. (2019) and Howard et al. (2020) use 40 000 K. From Table 3 the range in flare energy is $10^{33.5}$ to 10^{36} erg with a mean of $10^{34.5}$ erg, but these may be just lower limits.

6 CONCLUSION AND DISCUSSION

It is demonstrated that the periodic light variations seen in about 30–40 percent of A- and B-type stars is consistent with rotational modulation. The expected relationship between the estimated equatorial rotation velocity, v, and the projected rotation velocity, $v \sin i$, is confirmed in several effective temperature ranges.

The nature of the presumed starspots responsible for rotational modulation is not known. The idea of magnetic field generation in subsurface convective zones first postulated by Cantiello et al. (2009); Cantiello and Braithwaite (2011); Cantiello et al. (2011); Cantiello and Braithwaite (2019) seems to be quite promising. According to Cantiello and Braithwaite (2019), the largest effects are caused by a convective layer driven by second helium ionization. The amplitude of surface magnetic fields and their associated photometric variability are expected to decrease with increasing stellar mass and surface temperature, so that magnetic spots and their observational effects should be much harder to detect in late B-type stars. This is clearly not the case, since the fraction of late B-type stars showing rotational modulation is about the same as in A-type stars (Table 1). In fact, the fraction stays about the same at 30–40 percent for all stars in the upper main sequence.

Another problem is that sub-surface convection predicts the creation of bright spots. We know that spots on the Sun are dark, and this seems to be true of solar-type stars as well. Since rotational modulation is present for the full range of main sequence stars, there must be a transition between dark spots and bright spots around early F or late A. As a result, one might expect a decrease in the numbers of stars with rotational modulation in this spectral type range. This does not seem to be the case unless the transition is very sharp.

An alternative mechanism proposed many years ago involves the interaction between magnetic fields, convective flows and differential rotation. A dynamo cycle operating on differential rotation in stellar radiative interiors was described by Tout and Pringle (1995); Spruit (1999, 2002) and Maeder and Meynet (2004) (see also Braithwaite and Spruit 2017). In this theory, a magnetic instability in the toroidal field wound up by differential rotation replaces the role of convection in closing the field amplification loop in conventional dynamo theory. It is possible that completely stable radiative envelopes do not exist and that turbulence generated by differential rotation may lead to surface magnetic fields capable of forming conventional dark spots.

Examination of *TESS* A- and B-type stars has led to the detection of 57 new flare stars in addition to the 61 early-type flare stars already known from the *Kepler* mission. These new flare stars include some Ap and Am stars, with some stars being X-ray sources. If starspots are deemed to be present, in A- and B-type stars, then there should be no barrier to accepting that flares may be generated by magnetic reconnection, as in the Sun and cool stars. Indeed, it then becomes necessary to provide reasons why flares should *not* be generated in A- and B-type stars.

Cool dwarfs are plentiful, of course, but extremely faint. The apparent magnitudes of the *TESS* A-type stars are 4–10 mag with a median of 8.2 mag. A cool dwarf of comparable brightness, or even significantly fainter, will be one of the nearest stars and well documented. Using a catalogue of over one million cool dwarfs (Muirhead et al., 2018), it is found that a foreground cool dwarf within a radius of 2 arcmin cannot be the cause of the flares in A-type stars, which is not surprising. If the flare does not originate in a cool dwarf or the A star, then it must originate in an exotic faint object in the field or a physical companion to the A star.

As can be seen from Table 3, a typical A-star flare energy is about 10^{34}–10^{35} erg. These could be lower energy limits. While it is true that flares in cool dwarfs may attain such high energies on rare occasions, the question that needs to be asked is how many cool stars with flares in this energy range are likely to be observed by *TESS* within the same time interval. From nearly 25 000 cool stars observed by *TESS*, only a single M-type star out of 1228 flare stars was observed with a bolometric flare energy as high as $10^{34.7}$ erg (Günther et al., 2020). This does not, of course, imply that flares of even higher energy cannot occur in cool dwarfs. However, it does give an indication of the rarity of superflares in these stars. What needs to be examined is the probability of finding superflares in cool-star companions to 57 A-type stars with the observed energies in the same time interval and observed in the same way.

To answer this question, from the numbers presented by Günther et al. (2020), it can be deduced that superflares occur in about 0.004 percent of cool dwarfs observed in the first two months of the *TESS* mission. Most *TESS* stars are observed for only one or two sectors, so this is roughly comparable to the time span per star for the A- and B-type stars discussed here. Over this time interval, superflares are found in 1 percent of *TESS* A-type stars. This is much higher than the expected 0.004 percent and does not even include the multiple superflares in A-type stars which occur within several days, something which has

never been observed among cool flare stars. It seems that a physical cool star companion can be excluded as the source of the flares.

Superflares among F- and G-type giants have been discovered (Balona, 2012; Maehara et al., 2012). However, the A-type stars in which flares have been detected (Table 2) are bright and well observed. Spectroscopic observations give mostly early A types with no indication of F- or G-type giant companions. Since such companions would have luminosities similar to the A-type star, they should have been easily detected during spectroscopic classification. They would also have modified the photometric effective temperature estimates to cooler values, which is not the case. There is no evidence to suppose that flares on A-type stars originate in luminous F- or G-type physical companions either.

The above arguments show that a cool star or an F/G giant can be excluded as the source of flaring in A-type stars. There are two remaining possibilities: the flare arises in magnetic reconnection involving the A star and a close companion, or solely on the A star itself. Either way it means that a significant magnetic field must be present on the A star. This is, of course, what the rotational modulation observations suggest. We therefore return to the original problem regarding the presence of magnetic fields in radiative envelopes.

For further progress it will be important to design observations which might lead to resolving the problem of whether the spots are bright or dark. Further high-resolution spectroscopy of A- or B-type stars, as performed by Böhm et al. (2015) on Vega would be important to place limits on the size and distribution of the spots. It would also be important to obtain time-series spectroscopy on A- and B-type flare stars to determine possible interacting companions.

Above all, work on revising our existing notions of the physics in the outer layers of stars with radiative envelopes needs to be conducted. New ideas on how magnetic fields may be generated in such stars are required. The unexpected discoveries in pulsations in A- and B-type stars provide important clues. Perhaps a useful starting point is to determine what processes are required to generate low-frequency pulsations in δ Scuti stars or the enigmatic high frequencies in the B-type pulsating Maia variables.

ACKNOWLEDGMENTS

I wish to thank the National Research Foundation of South Africa for financial support. I also thank the *TESS* Asteroseismic Science Operations Center (TASOC).

Funding for the *TESS* mission is provided by the NASA Explorer Program. Funding for the *TESS* Asteroseismic Science Operations Centre is provided by the Danish National Research Foundation (Grant agreement no.: DNRF106), ESA PRODEX (PEA 4000119301) and Stellar Astrophysics Centre (SAC) at Aarhus University.

This work has made use of data from the European Space Agency (ESA) mission Gaia, processed by the Gaia Data Processing and Analysis Consortium (DPAC). Funding for the DPAC has been provided by national institutions, in particular the institutions participating in the Gaia Multilateral Agreement.

This research has made use of the SIMBAD database, operated at CDS, Strasbourg, France. Data were obtained from the Mikulski Archive for Space Telescopes (MAST). STScI is operated by the Association of Universities for Research in Astronomy, Inc., under NASA contract NAS5-2655.

CONFLICT OF INTEREST

I declare that there is no conflict of interest related to this work.

REFERENCES

Balona, L. A. (1994). Effective Temperature Bolometric Correction and Mass Calibration of O-F. MNRAS 268, 119–+

Balona, L. A. (2012). Kepler observations of flaring in A-F type stars. MNRAS 423, 3420–3429. doi:10.1111/j.1365-2966.2012.21135.x

Balona, L. A. (2013). Activity in A-type stars. MNRAS 431, 2240–2252. doi:10.1093/mnras/stt322

Balona, L. A. (2014). Low frequencies in Kepler δ Scuti stars. MNRAS 437, 1476–1484. doi:10.1093/mnras/stt1981

Balona, L. A. (2015). Flare stars across the H-R diagram. MNRAS 447, 2714–2725. doi:10.1093/mnras/stu2651

Balona, L. A. (2016). Rotational modulation in B stars observed by the Kepler K2 mission. MNRAS 457, 3724–3731. doi:10.1093/mnras/stw244

Balona, L. A. (2017). Starspots on A stars. MNRAS 467, 1830–1837. doi:10.1093/mnras/stx265

Balona, L. A. (2018). Gaia luminosities of pulsating A-F stars in the Kepler field. MNRAS 479, 183–191. doi:10.1093/mnras/sty1511

Balona, L. A. (2019). Evidence for spots on hot stars suggests major revision of stellar physics. MNRAS 490, 2112–2116. doi:10.1093/mnras/stz2808

Balona, L. A., Baran, A. S., Daszyńska-Daszkiewicz, J., and De Cat, P. (2015). Analysis of Kepler B stars: rotational modulation and Maia variables. MNRAS 451, 1445–1459. doi:10.1093/mnras/stv1017

Balona, L. A., Engelbrecht, C. A., Joshi, Y. C., Joshi, S., Sharma, K., Semenko, E., et al. (2016a). The hot γ Doradus and Maia stars. MNRAS 460, 1318–1327. doi:10.1093/mnras/stw1038

Balona, L. A., Handler, G., Chowdhury, S., Ozuyar, D., Engelbrecht, C. A., Mirouh, G. M., et al. (2019a). Rotational modulation in TESS B stars. MNRAS 485, 3457–3469. doi:10.1093/mnras/stz586

Balona, L. A., Holdsworth, D. L., and Cunha, M. S. (2019b). High frequencies in TESS A-F main-sequence stars. MNRAS 487, 2117–2132. doi:10.1093/mnras/stz1423

Balona, L. A. and Ozuyar, D. (2020a). Pulsation among TESS A and B stars and the Maia variables. MNRAS 493, 5871–5879. doi:10.1093/mnras/staa670

Balona, L. A. and Ozuyar, D. (2020b). TESS observations of Be stars: a new interpretation. MNRAS 493, 2528–2544. doi:10.1093/mnras/staa389

Balona, L. A., Švanda, M., and Karlický, M. (2016b). Differential rotation, flares and coronae in A to M stars. MNRAS 463, 1740–1750. doi:10.1093/mnras/stw2109

Blazère, A., Neiner, C., and Petit, P. (2016a). Discovery of a very weak magnetic field on the Am star Alhena. MNRAS 459, L81–L84. doi:10.1093/mnrasl/slw050

Blazère, A., Petit, P., Lignières, F., Aurière, M., Ballot, J., Böhm, T., et al. (2016b). Detection of ultra-weak magnetic fields in Am stars: β Ursae Majoris and θ Leonis. A&A 586, A97. doi:10.1051/0004-6361/201527556

Böhm, T., Holschneider, M., Lignières, F., Petit, P., Rainer, M., Paletou, F., et al. (2015). Discovery of starspots on Vega. First spectroscopic detection of surface structures on a normal A-type star. A&A 577, A64. doi:10.1051/0004-6361/201425425

Borucki, W. J., Koch, D., Basri, G., Batalha, N., Brown, T., Caldwell, D., et al. (2010). Kepler Planet-Detection Mission: Introduction and First Results. *Science* 327, 977–. doi:10.1126/science.1185402

Braithwaite, J. and Spruit, H. C. (2004). A fossil origin for the magnetic field in A stars and white dwarfs. Nature 431, 819–821. doi:10.1038/nature02934

Braithwaite, J. and Spruit, H. C. (2017). Magnetic fields in non-convective regions of stars. *Royal Society Open Science* 4, 160271. doi:10.1098/rsos.160271

Brown, T. M., Latham, D. W., Everett, M. E., and Esquerdo, G. A. (2011). Kepler Input Catalog: Photometric Calibration and Stellar Classification. AJ 142, 112. doi:10.1088/0004-6256/142/4/112

Buysschaert, B., Aerts, C., Bloemen, S., Debosscher, J., Neiner, C., Briquet, M., et al. (2015). Kepler's first view of O-star variability: K2 data of five O stars in Campaign 0 as a proof of concept for O-star asteroseismology. MNRAS 453, 89–100. doi:10.1093/mnras/stv1572

Cantiello, M. and Braithwaite, J. (2011). Magnetic spots on hot massive stars. A&A 534, A140. doi:10.1051/0004-6361/201117512

Cantiello, M. and Braithwaite, J. (2019). Envelope Convection, Surface Magnetism, and Spots in A and Late B-type Stars. ApJ 883, 106. doi:10.3847/1538-4357/ab3924

Cantiello, M., Braithwaite, J., Brandenburg, A., Del Sordo, F., Käpylä, P., and Langer, N. (2011). 3D MHD simulations of subsurface convection in OB stars. In *Active OB Stars: Structure, Evolution, Mass Loss, and Critical Limits*, eds. C. Neiner, G. Wade, G. Meynet, and G. Peters (Cambridge: Cambridge University Press), vol. 272 of *IAU Symposium*, 32–37. doi:10.1017/S174392131100994X

Cantiello, M., Langer, N., Brott, I., de Koter, A., Shore, S. N., Vink, J. S., et al. (2009). Sub-surface convection zones in hot massive stars and their observable consequences. A&A 499, 279–290. doi:10.1051/0004-6361/200911643

Charbonneau, P. (2014). Solar Dynamo Theory. ARA&A 52, 251–290. doi:10.1146/annurev-astro-081913-040012

Daszyńska-Daszkiewicz, J., Walczak, P., and Pamyatnykh, A. (2017). On possible explanations of pulsations in Maia stars. In *European Physical Journal Web of Conferences*. vol. 160 of *European Physical Journal Web of Conferences*, 03013. doi:10.1051/epjconf/201716003013

Evans, P. A., Osborne, J. P., Beardmore, A. P., Page, K. L., Willingale, R., Mountford, C. J., et al. (2013). VizieR Online Data Catalog: 1SXPS Swift X-ray telescope point source catalogue (Evans+ 2014). *VizieR Online Data Catalog* , IX/43

Evans, P. A., Page, K. L., Osborne, J. P., Beardmore, A. P., Willingale, R., Burrows, D. N., et al. (2019). VizieR Online Data Catalog: 2SXPS Swift X-ray telescope point source catalogue (Evans+, 2020). *VizieR Online Data Catalog* , IX/58

Froning, C. S., Kowalski, A., France, K., Loyd, R. O. P., Schneider, P. C., Youngblood, A., et al. (2019). A Hot Ultraviolet Flare on the M Dwarf Star GJ 674. ApJ 871, L26. doi:10.3847/2041-8213/aaffcd

Gaia Collaboration, Brown, A. G. A., Vallenari, A., Prusti, T., de Bruijne, J. H. J., Babusiaux, C., et al. (2018). Gaia Data Release 2. Summary of the contents and survey properties. *ArXiv e-prints*

Gaia Collaboration, Prusti, T., de Bruijne, J. H. J., Brown, A. G. A., Vallenari, A., Babusiaux, C., et al. (2016). The Gaia mission. A&A 595, A1. doi:10.1051/0004-6361/201629272

Głębocki, R. and Gnaciński, P. (2005). Systematic errors in the determination of stellar rotational velocities. In *13th Cambridge Workshop on Cool Stars, Stellar Systems and the Sun*, eds. F. Favata, G. A. J. Hussain, and B. Battrick. vol. 560 of *ESA Special Publication*, 571

Gontcharov, G. A. (2017). 3D stellar reddening map from 2MASS photometry: An improved version. *Astronomy Letters* 43, 472–488. doi:10.1134/S1063773717070039

Gray, R. O. (1991). The calibration of Stromgren photometry for A, F and early G supergiants.II. The F and early G supergiants. A&A 252, 237

Grigahcène, A., Antoci, V., Balona, L., Catanzaro, G., Daszyńska-Daszkiewicz, J., Guzik, J. A., et al. (2010). Hybrid γ Doradus-δ Scuti Pulsators: New Insights into the Physics of the Oscillations from Kepler Observations. ApJ 713, L192–L197. doi:10.1088/2041-8205/713/2/L192

Günther, M. N., Zhan, Z., Seager, S., Rimmer, P. B., Ranjan, S., Stassun, K. G., et al. (2020). Stellar Flares from the First TESS Data Release: Exploring a New Sample of M Dwarfs. AJ 159, 60. doi:10.

3847/1538-3881/ab5d3a

Hall, D. S. (1972). A T Tauri-Like Star in the Eclipsing Binary RS Canum Venaticorum. PASP 84, 323. doi:10.1086/129291

Howard, W. S., Corbett, H., Law, N. M., Ratzloff, J. K., Galliher, N., Glazier, A. L., et al. (2020). EvryFlare. III. Temperature Evolution and Habitability Impacts of Dozens of Superflares Observed Simultaneously by Evryscope and TESS. ApJ 902, 115. doi:10.3847/1538-4357/abb5b4

Jenkins, J. M., Twicken, J. D., McCauliff, S., Campbell, J., Sanderfer, D., Lung, D., et al. (2016). The TESS science processing operations center. In *Software and Cyberinfrastructure for Astronomy IV*. vol. 9913 of Proc. SPIE, 99133E. doi:10.1117/12.2233418

Koen, C. (2010). The "four sigma" limit for significant periodicities. Ap&SS 329, 267–271. doi:10.1007/s10509-009-0199-z

Kron, G. E. (1947). The Probable Detecting of Surface Spots on AR Lacertae B. PASP 59, 261. doi:10.1086/125964

Lo, K. K., Farrell, S., Murphy, T., and Gaensler, B. M. (2014). Automatic Classification of Time-variable X-Ray Sources. ApJ 786, 20. doi:10.1088/0004-637X/786/1/20

Luyten, W. J. (1949). A New Star of Large Proper Motion (L 726-8). ApJ 109, 532. doi:10.1086/145158

Maeder, A. and Meynet, G. (2004). Stellar evolution with rotation and magnetic fields. II. General equations for the transport by Tayler-Spruit dynamo. A&A 422, 225–237. doi:10.1051/0004-6361:20034583

Maehara, H., Shibayama, T., Notsu, S., Notsu, Y., Nagao, T., Kusaba, S., et al. (2012). Superflares on solar-type stars. Nature 485, 478–481. doi:10.1038/nature11063

Makarov, V. V. (2003). The 100 Brightest X-Ray Stars within 50 Parsecs of the Sun. AJ 126, 1996–2008. doi:10.1086/378164

Marino, A., Micela, G., Pillitteri, I., and Peres, G. (2006). X-ray variability of NGC 2516 stars in the XMM-Newton observations. A&A 456, 977–983. doi:10.1051/0004-6361:20054674

McQuillan, A., Mazeh, T., and Aigrain, S. (2013). Stellar Rotation Periods of the Kepler Objects of Interest: A Dearth of Close-in Planets around Fast Rotators. ApJ 775, L11. doi:10.1088/2041-8205/775/1/L11

McQuillan, A., Mazeh, T., and Aigrain, S. (2014). Rotation Periods of 34,030 Kepler Main-sequence Stars: The Full Autocorrelation Sample. ApJS 211, 24. doi:10.1088/0067-0049/211/2/24

Mestel, L. (1967). "Fossil" Magnetic Fields and the Oblique-Rotator Model. In *Magnetic and Related Stars*, ed. R. C. Cameron. 101

Moon, T. T. and Dworetsky, M. M. (1985). Grids for the determination of effective temperature and surface gravity of B, A and F stars using uvby-beta photometry. MNRAS 217, 305–315

Muirhead, P. S., Dressing, C. D., Mann, A. W., Rojas-Ayala, B., Lépine, S., Paegert, M., et al. (2018). A Catalog of Cool Dwarf Targets for the Transiting Exoplanet Survey Satellite. AJ 155, 180. doi:10.3847/1538-3881/aab710

Napiwotzki, R., Schoenberner, D., and Wenske, V. (1993). On the determination of effective temperature and surface gravity of B, A, and F stars using Stromgren UVBY beta photometry. A&A 268, 653–666

Nielsen, M. B., Gizon, L., Schunker, H., and Karoff, C. (2013). Rotation periods of 12 000 main-sequence Kepler stars: Dependence on stellar spectral type and comparison with v sin i observations. A&A 557, L10. doi:10.1051/0004-6361/201321912

Parker, E. N. (1955). Hydromagnetic Dynamo Models. ApJ 122, 293. doi:10.1086/146087

Pecaut, M. J. and Mamajek, E. E. (2013). Intrinsic Colors, Temperatures, and Bolometric Corrections of Pre-main-sequence Stars. ApJS 208, 9. doi:10.1088/0067-0049/208/1/9

Pedersen, M. G., Antoci, V., Korhonen, H., White, T. R., Jessen-Hansen, J., Lehtinen, J., et al. (2017). Do A-type stars flare? MNRAS 466, 3060–3076. doi:10.1093/mnras/stw3226

Petit, P., Lignières, F., Wade, G. A., Aurière, M., Alina, D., Böhm, T., et al. (2011). Weak magnetic fields of intermediate-mass stars. *Astronomische Nachrichten* 332, 943. doi:10.1002/asna.201111608

Reinhold, T., Reiners, A., and Basri, G. (2013). Rotation and differential rotation of active Kepler stars. A&A 560, A4. doi:10.1051/0004-6361/201321970

Robrade, J. and Schmitt, J. H. M. M. (2010). X-ray emission from the remarkable A-type star HR 8799. A&A 516, A38. doi:10.1051/0004-6361/201014027

Samus, N. N., Kazarovets, E. V., Durlevich, O. V., Kireeva, N. N., and Pastukhova, E. N. (2017). General catalogue of variable stars: Version GCVS 5.1. *Astronomy Reports* 61, 80–88. doi:10.1134/S1063772917010085

Savanov, I. S. (2019). Activity of A-type Star KIC 7047141. In *Physics of Magnetic Stars*, eds. D. O. Kudryavtsev, I. I. Romanyuk, and I. A. Yakunin. vol. 518 of *Astronomical Society of the Pacific Conference Series*, 195

Scargle, J. D. (1982). Studies in astronomical time series analysis. II - Statistical aspects of spectral analysis of unevenly spaced data. ApJ 263, 835–853. doi:10.1086/160554

Schmitt, J. H. M. M., Guedel, M., and Predehl, P. (1994). Spatially resolved X-ray and radio observations of Castor A+B+C. A&A 287, 843–851

Schmitt, J. H. M. M., Ioannidis, P., Robrade, J., Czesla, S., and Schneider, P. C. (2019). Superflares on AB Doradus observed with TESS. A&A 628, A79. doi:10.1051/0004-6361/201935374

Schröder, C. and Schmitt, J. H. M. M. (2007). X-ray emission from A-type stars. A&A 475, 677–684. doi:10.1051/0004-6361:20077429

Sikora, J., Wade, G. A., and Rowe, J. (2020). A spectroscopic test of the rotational modulation origin of periodic Kepler photometric variability of A-type stars. MNRAS 498, 2456–2471. doi:10.1093/mnras/staa2444

Smalley, B. and Dworetsky, M. M. (1993). The Atmospheric Parameters of A-Stars and F-Stars - Part One - Comparison of Various Methods. A&A 271, 515–+

Soubiran, C., Le Campion, J.-F., Brouillet, N., and Chemin, L. (2016). The PASTEL catalogue: 2016 version. A&A 591, A118. doi:10.1051/0004-6361/201628497

Spruit, H. C. (1999). Differential rotation and magnetic fields in stellar interiors. A&A 349, 189–202

Spruit, H. C. (2002). Dynamo action by differential rotation in a stably stratified stellar interior. A&A 381, 923–932. doi:10.1051/0004-6361:20011465

Strassmeier, K. G. (2009). Starspots. A&A Rev. 17, 251–308. doi:10.1007/s00159-009-0020-6

Tout, C. A. and Pringle, J. E. (1995). X-ray coronae from dynamos in young Ae/Be stars. MNRAS 272, 528–530. doi:10.1093/mnras/272.3.528

Voges, W., Aschenbach, B., Boller, T., Bräuninger, H., Briel, U., Burkert, W., et al. (1999). The ROSAT all-sky survey bright source catalogue. A&A 349, 389–405

Voges, W., Aschenbach, B., Boller, T., Brauninger, H., Briel, U., Burkert, W., et al. (2000). Rosat All-Sky Survey Faint Source Catalogue. IAU Circ. 7432, 3

Švanda, M. and Karlický, M. (2016). Flares on A-type Stars: Evidence for Heating of Solar Corona by Nanoflares? ApJ 831, 9. doi:10.3847/0004-637X/831/1/9

Yanagida, T., Ezoe, Y., Kawaharada, M., Kokubun, M., and Makishima, K. (2007). Large X-ray Flares from B-Type Stars, HD261902 and HD47777, in NGC2264 Observed with CHANDRA. In *Active OB-Stars: Laboratories for Stellare and Circumstellar Physics*, ed. A. T. Okazaki, S. P. Owocki, & S. Stefl. vol. 361 of *Astronomical Society of the Pacific Conference Series*, 533

Yanagida, T., Ezoe, Y.-I., and Makishima, K. (2004). X-Ray Flares from a Late B-Type Star, HD 38563S, in NGC 2068 Observed with Chandra X-Ray Observatory. PASJ 56, 813–818